Original Research Article

Naringenin nanocrystals for improving anti-rheumatoid arthritis activity

Check for updates

Guangshuai Zhang[a], Guangyuan Sun[a], Haishan Guan[a], Mo Li[b], Yanhua Liu[c], Baocheng Tian[d], Zhonggui He[a], Qiang Fu[a,e,]*

[a] *Wuya College of Innovation, Shenyang Pharmaceutical University, Shenyang 110016, China*
[b] *Liaoning Institute for Drug Control, Shenyang 110016, China*
[c] *School of Pharmacy, Ningxia Medical University, Yinchuan 750004, China*
[d] *School of Pharmacy, Binzhou Medical University, Yantai 264003, China*
[e] *Sihuan Pharmaceutical Holdings Group Ltd., Beijing 100013, China*

ARTICLE INFO

ABSTRACT

Naringenin (NAR) is recognized for its anti-inflammatory activity. However, the clinical application of NAR is limited by low bioavailability, which is attributed to its poor aqueous solubility. In this study, we aimed to improve the therapeutic efficacy of NAR by formulating it into nanocrystals (NCs) via wet milling. The obtained NARNCs exhibited superior dissolution behaviors, increased cellular uptake, and enhanced transcellular diffusion relative to those of bulk NAR. Oral administration of NARNCs also significantly improved bioavailability in rats. In addition, the NARNCs effectively improved rheumatoid arthritis treatment in collagen-induced arthritic rats by reducing inflammatory cell infiltration and synovial damage. These results indicate that NARNCs provides a promising strategy for rheumatoid arthritis treatment.

1. Introduction

Rheumatoid arthritis (RA) is an autoimmune disease [1]. With RA, the joints progressively become unable to move, inflicting significant suffering for patients. The World Health Organization reports that 80% of individuals with RA have severe disabilities. Moreover, RA not only affects livelihoods but also increases the socioeconomic burden [2]. Several drugs have been used for the treatment of RA, such as nonsteroidal anti-inflammatories, glucocorticoids, and biological drugs. However, these drugs also cause infections, cardiovascular side effects, delayed bone healing, and other adverse reactions [3–5]. Therefore, new strategies for RA treatment need to be developed.

Natural compounds have recently drawn widespread attention because of their immunomodulatory properties and potential to treat inflammatory diseases [2]. Naringenin (NAR), which is mainly found in citrus fruits and tomatoes,

---

is a group of compounds with antioxidative and anti-inflammatory properties and other biological activities [6,7]. However, the poor water solubility and low dissolution rate of NAR considerably limit its use [8]. To address these problems, several systems have been developed, including liposomes [9], emulsions [10], solid dispersions [11], nanoparticles [12], and cosolvents [13]. However, the positive effects of these systems are compromised by low drug loading, potential toxicity, high cost, and other disadvantages [14].

Nanocrystals (NCs) are submicron colloidal dispersions stabilized by macromolecular polymers [15]. Colloidal systems are characterized by high loading, negligible side effects, and low costs. They can also improve the saturated solubility and dissolution rate for water-insoluble substances because of the increased specific surface area [16]. Generally, NCs can be prepared using two methods: the bottom-up method (building up nanoprecipitation from dissolved molecules) and the top-down method (breaking up large particles into nanosizes) [17]. Owing to the absence of an organic solvent, the top-down technique is more widely used than the bottom-up approach. Wet-media grinding is the most frequently applied technique because of its ease of scaling up [18].

This study mainly aimed to prepare stable NARNCs by wet milling and to explore their potential application in the treatment of RA. The physiochemical characteristics, physical stability, and dissolution performances of the NARNCs were assessed. Cellular uptake and transport in the NARNCs were subsequently evaluated based on Caco-2 cell models. Finally, the *in vivo* pharmacokinetic behaviors and anti-inflammatory effects of NARNCs were studied. The results of this study provide new insights into RA treatment.

2. Materials and methods

2.1. Materials

NAR was obtained from Wuhan Yuancheng Gongchuang Technology Co., Ltd. (Wuhan, China). Minimum Eagle's medium/Earle's balanced salt solution (MEM/EBSS) was purchased from Hyclone Laboratories, Inc. (Utah, USA). Lutrol® poloxamer 407 (F127) and Cremophor® EL were supplied by BASF Co., Ltd. (Shanghai, China). 3-(4,5-Dimethylthiazol-2-yl)−2,5-diphenyltetrazolium bromide (MTT), 2′,7′-dichlorodihydrofluorescein diacetate (DCFH–DA), phosphate-buffered saline (PBS), penicillin, and streptomycin sulfate were purchased from Dalian Meilun Biotechnology Co., Ltd. (Dalian, China). Dulbecco's modified Eagle's medium (DMEM), nonessential amino acid, sodium pyruvate, and fetal bovine serum (FBS) were provided by Gibco (Carlsbad, CA). BCA assay kits were supplied by Shenyang Dingguo Biotechnology Co., Ltd. (Shenyang, China). β-glucuronidase and SiO_2 were purchased from Sigma-Aldrich (Missouri, USA). The Caco-2 cell line and RAW 264.7 cell line were supplied by the American Type Culture Collection (Manassas, USA). Bovine Type II Collagen and incomplete Freund's adjuvant were purchased from Chondrex (Washington DC, USA). Enzyme-linked immunosorbent assay (ELISA) kits for interleukin-1β (IL-1β), interleukin-6 (IL-6), and tumor necrosis

factor-α (TNF-α) were purchased from ABclonal Technology Co., Ltd. (Wuhan, China). All other reagents were of analytical grade.

2.2. Preparation of the NARNCs

The NARNCs were prepared using a planetary ball mill (Nanjing Chishun Science and Technology Co., Ltd., Nanjing, China). Under magnetic stirring, 2 g of NAR and 0.2 g of F127 were dispersed in 20 ml of water. The aforementioned dispersion was transferred to a grinding bowl containing zirconia beads (Ø 0.5 mm). The samples were ultimately milled at 30 Hz for 125 min, with intervals of 3 min after every milling period of 5 min.

The aqueous NARNCs were lyophilized using a DRC-1000REC freeze dryer (Tokyo Rikakikai Co., Ltd., Japan) for physicochemical characterization. For primary drying, the shelf inlet temperature was initially set to −40 °C, which was maintained for 5 h. It was then increased to −20 °C, maintained at the same temperature for 12 h. Finally, secondary drying was conducted at 30 °C for 6 h.

The NAR solution (NAR Sol) was used as a control in cell and animal studies. NAR Sol was prepared by adding 1 g of NAR to 20 ml of the cosolvent Cremophor® EL-ethanol (1:1, v/v).

2.3. Characterization of NARNCs

2.3.1. Particle sizes and zeta potentials of NARNCs
The particle sizes, polydispersity indexes (PDIs), and zeta potentials of NARNCs were characterized using a Zetasizer Nano ZS90 (Malvern Instruments Ltd., UK).

2.3.2. Transmission electron microscopy (TEM)
The morphology of the NARNCs was characterized using the HT-7700 instrument (Hitachi, Japan). After dilution, NARNCs were dropped onto copper grids (Beijing Zhongjingkeyi Technology Co., Ltd., China) with 200-mesh carbon membranes and then dried.

2.3.3. Differential scanning calorimetry (DSC)
To characterize the crystal form of NARNCs, DSC was performed using the DSC1 instrument (Mettler-Toledo International Inc., Switzerland). About 6 mg of the samples were sealed in an alumina crucible and heated from 30 to 300 °C at a linear heating rate of 10 °C/min.

2.3.4. Powder X-ray diffraction (PXRD)
To examine the crystallinity of NARNCs, PXRD analysis was performed using the X'pert Pro-MPD X-ray diffractometer (PANalytical B.V., Netherlands) under the following conditions: scanning speed, 5°/min; 2θ range, 5°−55°, and scanning increment, 0.02°

2.3.5. Fourier transform infrared spectroscopy (FTIR)
The interaction between NAR and F127 was analyzed by FTIR using the Bruker IFS 55 FTIR spectrometer (Bruker Ltd., Switzerland) in the 4000–500 cm^{-1} wavelength range with a resolution of 2 cm^{-1} scannings. The samples were compressed into tablets with potassium bromide.

2.3.6. Raman spectroscopy

The interaction between NAR and F127 was further analyzed by Raman spectroscopy. The spectra of the samples were obtained using a Renishaw inVia Raman microscope (Renishaw, Gloucestershire, United Kingdom) under the following conditions: wavelength range, 500–3500 cm^{-1}; laser power density, 100 Mw/µm^2, and integration time, 5 s.

2.4. Physical stability evaluation

The physical stability of the NARNCs was evaluated at 4 °C, 25 °C, and 37 °C for 30 d The samples were collected at 0, 1, 3, 5, 10, 15, 20, and 30 d, and the particle sizes were determined as described in Section 2.3.1.

2.5. In vitro dissolution testing

Dissolution testing of NARNCs was performed in a ZRS-8 G dissolution apparatus (Tianda Tianfa Technology Co., Ltd., China) with a paddle speed of 50 rpm and using 900 ml of water as the medium. NAR, the physical mixture (PM), NARNCs, and NAR Sol (equivalent to 30 mg of NAR) were dissolved in the medium, which was kept constant at 37 °C. Subsequently, 5 ml of the sample was taken out at 5, 10, 20, 30, 45 and 60 min and immediately replaced with fresh water. After filtering with a 0.22 µm microporous filter, NAR was quantitatively analyzed by high performance liquid chromatography (HPLC) as described in supply.

2.6. Cell studies

2.6.1. Cell culture

Caco-2 cells were grown in MEM/EBSS supplemented with 10% (v/v) FBS, 1% (w/v) penicillin, 1% (w/v) streptomycin, 1% (w/v) sodium pyruvate, and 1% (w/v) nonessential amino acid. RAW 264.7 cells were cultured in DMEM containing 10% (v/v) FBS, 1% (w/v) penicillin, and 1% (w/v) streptomycin. Both cells were cultured at 37 °C with 90% relative humidity and 5% CO$_2$ supply.

2.6.2. Cytotoxicity analysis

Cytotoxicity evaluation was conducted by MTT assay. Caco-2 cells were seeded in 96-well plates (NEST Biotechnology Co. Ltd., China) at a density of 5×10^3 cells/well and then cultured for 72 h. After the cells were exposed to NAR, NARNCs, and NAR Sol for 12 h, the medium was replaced with 200 µl of the MTT solution (0.5 mg/ml in PBS), and the cells were incubated for 4 h. The supernatant was then discarded, and dimethyl sulfoxide (200 µl/well) was added to dissolve the formazan crystals. The absorption was ultimately measured at 570 nm by using a Varioskan Flash multiplate reader (ThermoFisher, Massachusetts, USA), and the relative cell viability was calculated.

2.6.3. Cellular uptake

Caco-2 cells (5×10^3 cells per well) were seeded in 24-well plates (NEST Biotechnology Co. Ltd., Wuxi, China) to evaluate cellular uptake. In Week 1, the medium was changed every 2 d The medium was refreshed daily until Day 14. The Caco-2 cells

were then pretreated with fresh PBS at 37 °C for 0.5 h. The cells were cultured with 100 µM of the NAR suspension, NARNCs, and NAR Sol for different durations (0.25, 0.50, 0.75, 1.00, 1.50, and 2.00 h). The Caco-2 cells were subsequently washed with PBS and collected with 300 µl of water. The samples were disrupted in the SCIENTZ-IID Ultrasonic Homogenizer (Ningbo Scientz Biotechnology Co., Ltd., Ningbo, Zhejiang). Total protein was quantified using a BCA assay kit.

To analyze the amount of NAR, the samples were hydrolyzed by β-glucuronidase [19]. About 200 µl of the cell sample was first deproteinized by vortexing with 600 µl of ethanol and then centrifuged 11 000 g for 5 min. The supernatant was dried and resuspended with PBS. The pH of the sample was subsequently adjusted to 4.5–5.5 and incubated with 25 µl β-glucuronidase (sodium acetate buffer, 30 mg/ml) and 12.5 µl of ascorbic acid (10% w/v) in the dark at 37 °C for 1 h. The samples were then incubated with ethyl acetate, followed by vortexing for 5 min. After centrifugation at 11 000 g for 5 min, the supernatant was collected, evaporated, redissolved in methanol, and determined by HPLC in accordance with the method described in Supplementary Material.

2.6.4. Caco-2 cell permeability

For transport studies, Caco-2 cells (2×10^4 cells per well) were cultured on Transwell® 3402 filters (Corning Costar, USA). The medium was refreshed daily during the cultivation. After differentiation for 21 d, the transepithelial electrical resistance (TEER) was measured with the Millicell ERS cell resistance meter (Merck Millipore, USA). TEER values higher than 250 Ω/cm^2 were used.

Caco-2 cells were first equilibrated with PBS at 37 °C. Subsequently, 100 µM NAR crude suspension, NARNCs, and NAR Sol were added to the apical side. During incubation, 300 µl of the sample was removed from the lower chambers at different time points (15, 30, 45, 60, 90, and 120 min), and 300 µl of fresh PBS was added. The samples were determined by HPLC as described in Supplementary Material. The apparent permeability coefficient (P$_{app}$) was calculated using the following formula:

$$P_{app} = \frac{dQ}{dt} \times \frac{1}{A \times C_0}$$

where dQ/dt is the flux of NAR, A is the filter membrane area (cm^2), and C_0 is the initial concentration of NAR.

2.6.5. In vitro anti-inflammatory activity

Caco-2 cells were cultured in Transwell® 3402 as described in 2.6.4. On Day 21, RAW 264.7 cells (2×10^5 cells/well) were cultured in the lower compartments with DMEM for 12 h. The medium in the lower compartments was changed to 50 µg/ml SiO$_2$ DMEM for 4 h incubation and finally replaced with PBS [20,21]. Subsequently, 100 µM NAR suspension, NARNCs, and NAR Sol were added to the apical side for 2 h incubation. The samples were subsequently collected from the basolateral chambers and the levels of TNF-α, IL-1β, and IL-6 were measured using ELISA kits. The RAW 264.7 cells were washed and then treated with 10 µM DCFH–DA in a dark environment for 30 min to determine the intracellular reactive oxygen

species (ROS) levels. The cells were then washed with PBS to remove free DCFH–DA. Fluorescence signals were recorded using a Varioskan Flash multiplate reader, and fluorescence microscopy images were acquired using an IX71 inverted fluorescence microscope (Olympus Corporation, Tokyo, Japan).

2.7. Animal studies

All animal experiments were approved by the Animal Ethics Committee of Shenyang Pharmaceutical University and performed in accordance with the Guidelines for the Care and Use of Laboratory Animals [22]. Male Sprague–Dawley rats weighing 200–220 g were purchased from Shenyang Changsheng Animal centre (Shenyang, China).

2.7.1. Pharmacokinetics

For pharmacokinetic studies, the rats were fasted for 12 h before the experiments, and food was reoffered 6 h post-dosing. The rats were randomly divided into three groups ($n = 6$), which were orally administered with NAR suspension, NARNCs, and NAR Sol at a single dose of 50 mg/kg). Blood samples were collected in heparinized tubes at 0.083, 0.25, 0.50, 0.75, 1, 2, 4, 6, 8, 10, 12 and 24 h and centrifuged immediately at 11 000 g for 3 min. Plasma samples were then stored at $-20\,°C$ until analysis.

All plasma samples (100 µl) were incubated with β-glucuronidase (50 µl) at 37 °C for 2 h [23] and then subjected to liquid-liquid extraction. About 50 µg/ml apigenin was used as the internal standard solution. After the enzyme treatment, the samples were vortexed with 20 µl internal standard solution and extracted with 1 ml ethyl acetate. The mixtures were vortexed for 3 min and then centrifuged at 3000 g for 5 min. The supernatants were collected and evaporated to dryness under a gentle stream of nitrogen at 37 °C. The residues were reconstituted in 100 µl of methanol-water (5:95, v/v) solution and analyzed by HPLC as described in Supplementary Material.

2.7.2. In vivo anti-inflammatory activity

A rat collagen-induced arthritis (CIA) model was established using the method published in a previous study [24]. About 2 mg/ml of bovine type II collagen and Freund's incomplete adjuvant (1:1, v/v) were mixed and emulsified. The emulsified reagents were injected subcutaneously into the tail base of the rats on Day 1 (200 µl) and Day 7 (100 µl). On Day 21, a total of 25 CIA rats were equally divided into five groups: the control group (untreated with CIA), the CIA model group (untreated), the NAR (suspension) group, the NARNC group, and the NAR Sol group. The daily oral dose was 50 mg/kg, and the first day the dose was administered was regarded as Day 0. The thicknesses of the hind paws, arthritis index scores, and body weights of the rats were recorded every 3 d On Day 30, rats were sacrificed, and ankle joints were collected. Dissected joints were fixed in 4% paraformaldehyde and decalcified completely in a formalin-EDTA solution. Tissues were sliced into 5 µm sections cut and then stained with hematoxylin-eosin. The stained sections were photographed using the Ni-U fluorescence microscope (Nikon, Japan).

2.8. Statistical analysis

The two-tailed unpaired Students' t-test was used to evaluate whether the difference between the two groups was significant. $*P < 0.05$, $**P < 0.01$, $\#P < 0.001$, and $\#\#P < 0.0001$.

3. Results and discussion

3.1. Preparation of NARNCs

NARNCs were prepared using a planetary ball mill. The grinding time and stabilizer concentrations were critical to determining particle sizes and PDIs [14,25]. Thus, the milling time and the amount of stabilizer were determined. The effects of milling time on particle sizes are shown in Fig. 1A. In the initial stages, the particle sizes and PDIs decreased rapidly with an increase in time. The particle size was 282.5 nm, and PDI was 0.088 after the particles were milled for 125 min. Subsequently, the reduction in particle size gradually became insignificant. The particles were milled again for another period of 50 min, after which the particle size decreased to 259.5 nm, whereas the PDIs increased significantly to 0.175. To prevent agglomeration, different concentrations of F127 were investigated. The results (Fig. 1B) indicated that NARNCs stabilized by 0.6% F127 (w/v) had the smallest particle size and highest best dispersion state. Therefore, the optimal NARNCs were stabilized using 0.6% (w/v) F127 and milled for 125 min. The particle sizes, PDIs and zeta potential were 274.3 ± 3.3 nm, 0.028 ± 0.023 and $-12.4 ± 0.4$ mV, respectively. The physical stability of the NARNCs was evaluated at 4 °C, 25 °C, and 37 °C. The results are shown in Fig. 1D and S1. No significant change in the particle size of the NARNCs ($P > 0.05$) was observed at 4 °C and 25 °C within 30 d However, the particle size slightly increased to 304 nm when the NARNCs were stored at 37 °C for 20 d because of Ostwald ripening.

In the initial stages of grinding (0 to 125 min), the particle sizes and PDIs decreased rapidly with an increase in milling time because the stabilizers could quickly cover the surface of NAR and facilitate the breakage of crude particles into nanoparticles [14]. However, in the late stages (125 to 175 min), the excess energy due to over-grinding could also disrupt repulsive forces, induce the aggregation of small particles, and affect the physical stability of the system [26]. The concentration of the stabilizers was also a critical factor for particle-size distribution and the dispersed state because stabilizers at a proper concentration (0.6% F127) could cover the surface of the drug crystals and prevent aggregation. If the stabilizers were insufficient (0.4% F127), nanoparticles with high free energy would agglomerate. By contrast, an excessive number of stabilizers would promote Ostwald ripening, and smaller particles with higher solubility would dissolve and recrystallize to form larger particles [27].

3.2. Characterization of NARNCs

3.2.1. Morphology

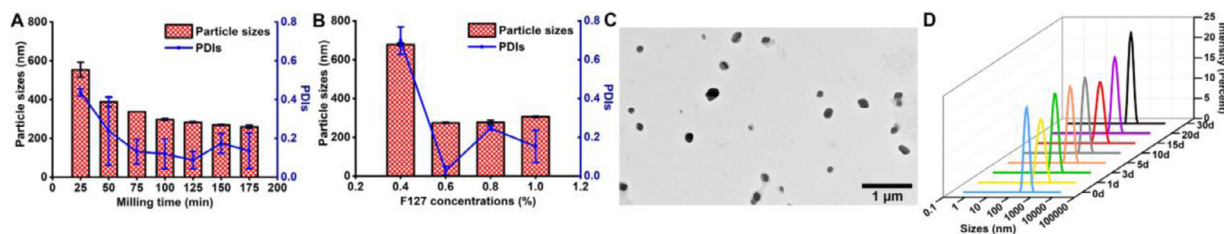The shape of NCs may affect physical, chemical, and biological properties [28]. Therefore, the surface morphology

Fig. 1 – Effects of (A) milling time and (B) F127 concentrations on particle size and PDIs (data are mean ± SD, n = 3). (C) TEM and (D) physical stability (particle sizes) of NARNCs at 25 °C for 30 d
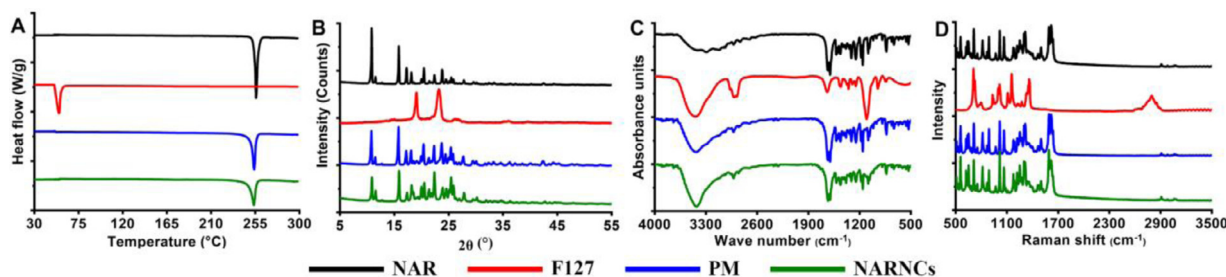

Fig. 2 – Physical characterization of bulk NAR, F127, PM, and NARNCs: (A) DSC, (B) PXRD, (C) FTIR, and (D) Raman spectroscopy.

of the NARNCs was observed by TEM. As shown in Fig. S2, untreated NAR is rod-shaped. After wet milling, the large NAR crystals were broken into irregularly block-shaped NARNCs (Fig. 1C).

3.2.2. Crystalline state

The conversion of a crystalline form during milling may cause quality problems. Therefore, the crystalline structure of NARNCs was examined using DSC and PXRD. In Fig. 2, the DSC thermograms (Fig. 2A) show that crude NAR has an endothermic peak at 255.70 °C, whereas F127 does not. The melting peak in the PM was slightly reduced and broadened, which could be attributed to the presence of F127 [29]. However, no significant difference was found between the PM and NARNCs, suggesting that the crystal form was unchanged during grinding. PXRD analysis was also conducted to confirm the crystalline state. The results are shown in Fig. 2B. NAR showed sharp characteristic diffraction peaks at 2θ values of 10.83°, 15.85°, 17.24°, 18.15°, 20.46°, 22.40°, 23.80°, 24.50°, 25.50° and 27.81° NARNCs still had all the above peaks, indicating that the crystal form of NAR was maintained after milling.

3.2.3. Intermolecular interactions

The molecular interaction between NAR and F127 was examined by FT-IR and Raman analysis. The FTIR spectra (Fig. 2C) of bulk NAR exhibited characteristic peaks at 3294 cm^{-1} (the OH stretching vibration), 3057 cm^{-1} (the aromatic stretching vibration of C–H), 1631 cm^{-1} (the C=O stretching vibrations), and 1014 cm^{-1} (the C–O stretching). These characteristic peaks showed no significant change in the spectra of PM and NARNCs, demonstrating that no hydrogen bond was formed between NAR and F127. This result was confirmed by Raman spectroscopy. NAR showed
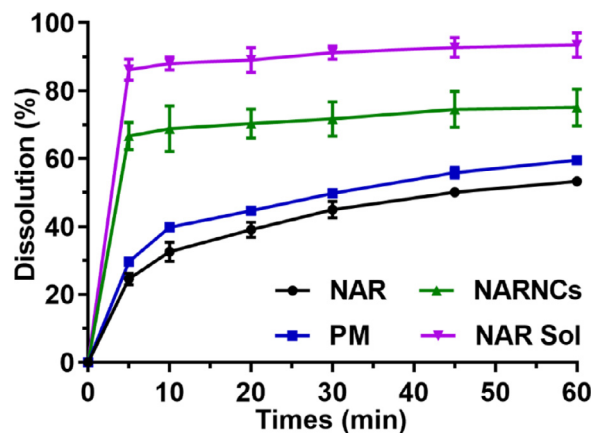

Fig. 3 – Dissolution profiles of NAR, PM, NARNCs, and NAR Sol in water (mean ± SD, n = 3).

characteristic peaks at 555, 636, 650, 711, 815, 890, 1016, 1315, 1591, and 1618 cm^{-1} (Fig. 2D). These characteristic peaks also existed in the PM and NARNCs. Together, these findings indicate that no obvious interaction occurred between NAR and F127.

3.3. In vitro dissolution

NAR is a poorly water-soluble drug, and its low dissolution rate limits its oral bioavailability and therapeutic effects [30]. Thus, dissolution testing was conducted to evaluate whether the dissolution of NAR improved after nanonization. As shown in Fig. 3, only 53.29% ± 0.83% and 59.54% ± 0.38% of NAR were dissolved from crude NAR and the PM, respectively, after 60 min. However, after nanonization,

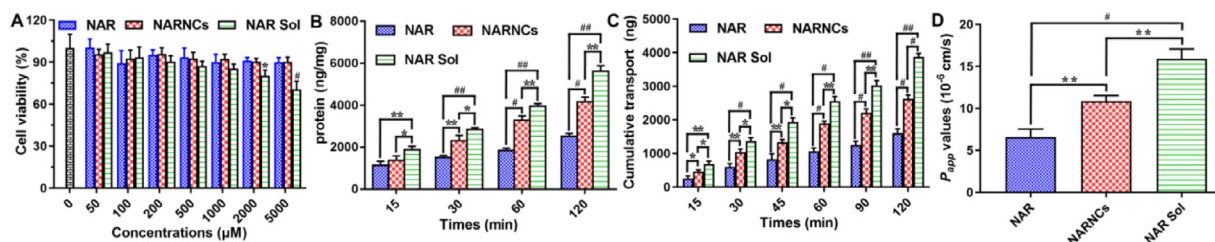**Fig. 4 – (A)** Degrees of cytotoxicity of NAR, NARNCs, and NAR Sol (mean ± SD, $n = 6$). **(B)** Amounts of NAR in the Caco-2 cells after incubation with the NAR suspension, NARNCs, and NAR Sol over different durations. **(C)** Cumulative transport of NAR suspension, NARNCs, and NAR Sol. **(D)** P_{app} values of NAR suspension, NARNCs, and NAR Sol across Caco-2 cell monolayers. Data are shown as mean ± SD ($n = 3$), *$P < 0.05$, **$P < 0.01$, #$P < 0.001$, and ##$P < 0.0001$.

the dissolution rate increased significantly, as verified by the NARNC dissolution rate of 75.05% ± 5.37% in water after 60 min. The improved dissolution rate of NARNCs could be attributed to the decrease in particle size. In accordance with the Noyes–Whitney equation and the Prandtl equation, a smaller particle size contributes to a decrease in the diffusion distance, an increase in the specific surface area, and saturated solubility, significantly improving the dissolution rate. Moreover, NAR Sol showed the highest dissolution rate among the four groups. The reason was that NAR already existed in a molecular state for NAR Sol.

3.4. Cell studies

3.4.1. Cytotoxicity analysis
Cytotoxicity was evaluated using MTT assays. As shown in Fig. 4A, NAR and NARNCs exert no significant effects on the viability of the Caco-2 cells within the tested concentration range of 50–5000 µM, indicating their good biocompatibility. However, cell viability in the NAR Sol group gradually decreased with an increase in concentration. Specifically, when the concentration exceeded 2000 µM, apparent cytotoxicity ($P < 0.05$) was exhibited, which could be attributed to the high concentrations of Cremophor® EL and ethanol.

3.4.2. Cellular uptake of NAR
The cellular uptake of NARNCs was further evaluated, with NAR suspension and NAR Sol as controls. Within 2 h, the internalization of all formulations was time-dependent (Fig. 4B). The absorption of NAR Sol was higher than that of NARNCs, which could be explained by the quick passive diffusion of free NAR. In addition, bulk NAR exhibited the least uptake. After nanonization, the internalization of NARNCs was significantly improved.

3.4.3. Transport of NAR
The permeability of NAR was evaluated in an intestinal epithelium model simulated by Caco-2 cell monolayers. As shown in Fig. 4C and 4D, the transport rate of NARNCs is significantly higher than that of bulk NAR ($P < 0.01$), indicating that nanonization can improve the permeability of NAR. P_{app} was also calculated to compare the permeability of the NAR suspension, NARNCs, and NAR Sol. As described in Fig. 4D,

Table 1 – Pharmacokinetic parameters of NAR after oral administration to rats (mean ± SD, $n = 6$).

Pharmacokinetic Parameters	NAR	NARNCs	NAR Sol
C_{max} (µg/ml)	3.92 ± 1.93 **	7.63 ± 0.44	16.31 ± 7.81 *
T_{max} (h)	0.5	0.5	0.5
$T_{1/2}$ (h)	10.86	4.76	7.58
$AUC_{0–24\,h}$ (µg·h/ml)	25.94 ± 10.19**	45.57 ± 7.36	58.92 ± 6.84 *

* $P < 0.05$. ** $P < 0.01$ *versus* NARNCs as the control.

the P_{app} value of the NARNCs (10.86×10^{-6} cm/s) was 1.65-fold that of the NAR suspension (6.58×10^{-6} cm/s) but smaller than that of NAR Sol (15.91×10^{-6} cm/s). This result was similar to the dissolution performance, indicating that the increased dissolution rate could enhance transcellular diffusion.

3.4.4. Studies on the in vitro anti-inflammatory effects of NAR
The SiO$_2$-induced RAW 264.7 inflammation model was established to assess the anti-inflammatory effects of NAR. As shown in Fig. 5A, after NAR treatment, the levels of THF-α ($P < 0.05$), IL-1β ($P < 0.001$), IL-6 ($P < 0.01$), and ROS ($P < 0.01$) are significantly reduced, indicating the superior anti-inflammatory activity of NAR. All inflammatory cytokine levels markedly decreased in the NARNC group relative to those in the NAR suspension group. The enhanced anti-inflammatory activity could be attributed to the increased permeability. In addition, the NAR Sol exerted superior anti-inflammatory effects to those of NARNCs, but the difference was not apparent ($P > 0.05$).

3.5. Animal studies

3.5.1. Pharmacokinetic studies
To examine the *in vivo* behaviors of NARNCs, pharmacokinetic studies in rats were conducted. The plasma concentration of NAR was measured by HPLC, and the results are shown in Fig. 6 and Table 1. C_{max} and $AUC_{0–24\,h}$ of the NAR crude suspension were 3.92 ± 1.93 µg/ml and 25.94 ± 10.19 µg·h/ml, which were considerably lower than ($P < 0.01$) those of NARNCs (7.63 ± 0.44 µg/ml and 45.57 ± 7.36 µg·h/ml), demonstrating that the oral absorption of NAR was potentially
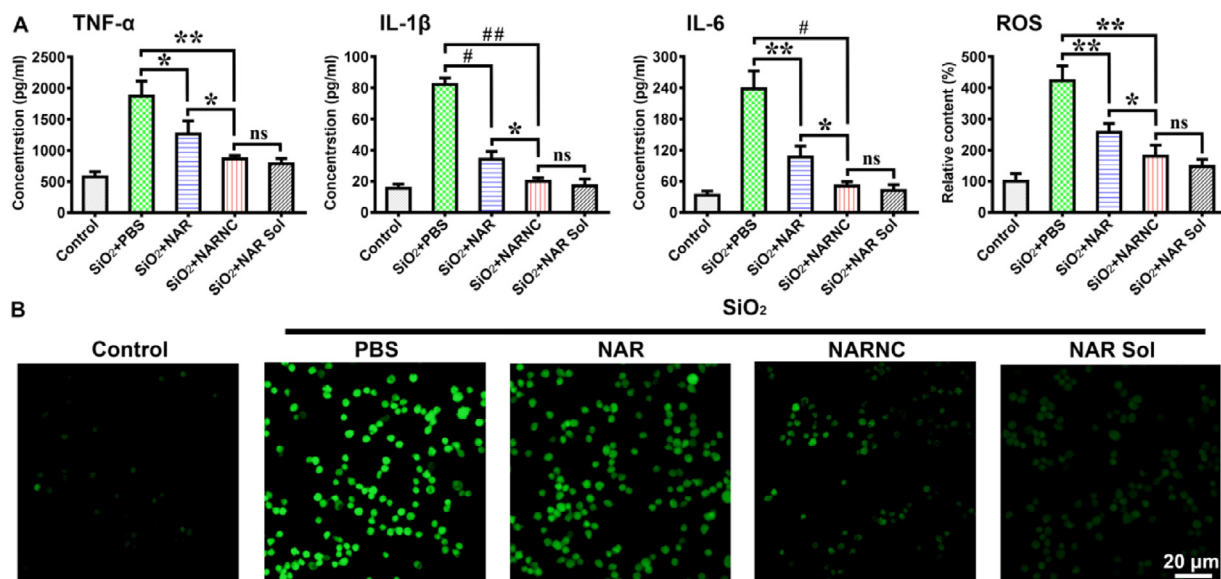
Fig. 5 – *In vitro* anti-inflammatory effects of NAR. (A) Concentrations of inflammatory cytokines. Data are shown as mean ± SD ($n = 3$), *$P < 0.05$, **$P < 0.01$, #$P < 0.001$, and ##$P < 0.0001$. (B) Fluorescence images of intracellular ROS stained with DCFH–DA. Bar: 20 µm.
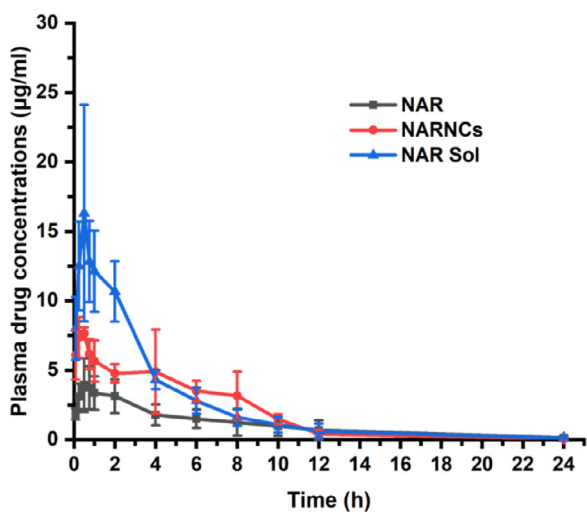

Fig. 6 – Plasma drug concentration profiles of NAR after oral administration.

improved after nanonization. Meanwhile, NAR Sol exhibited the highest absorption because it was in the molecular state and did not need to be dissolved.

3.5.2. *Therapeutic efficacy of NAR in vivo*

To confirm the anti-inflammatory effects of NAR, a rat CIA model was established. Fig. 7A presents the schematic of CIA rat model establishment and treatment programs. Paw thickness was smaller in the NAR group than in the saline group; however, no significant difference was found (Fig. 7B). Meanwhile, the NARNC group showed significantly less swelling of the hind legs, compared with the saline group ($P < 0.05$). The arthritis scores also indicated that nanonization could improve the anti-arthritis efficacy of NAR.

As shown in Fig. 7C, the rats treated with NAR suspension have hind paws similar to those of untreated rats; however, the rats treated with NARNCs have significantly reduced swelling. Histological examination of the hind limbs was also conducted (Fig. 7C). It showed that the joints of the rats in the saline group were infiltrated by a large number of inflammatory cells, and the synovium was severely damaged. The rats treated with NAR showed relatively low inflammatory cell infiltration and occasional synovial damage. By contrast, the NARNC group exhibited the mildest inflammation. The NARNC group showed the least inflammatory cell infiltration and the most extensive synovial protection among the groups. The Sol group showed similar anti-inflammatory effects with those of the NARNC group but also had significant weight loss (Fig. 7B) and liver toxicity (Fig. S3).

Aqueous solubility is a key parameter affecting the oral absorption of a drug [31]. However, most existing drugs and chemical entities have poor water solubility [28]. For the formulation of these drugs, several formulation strategies have been developed [32,33]. Among these, the solution is the simplest and its cost is the lowest [34,35]. However, a large number of surfactants and/or organic solvents have to be added to improve its solubility. For drugs used for acute diseases, short-term administration can alleviate the symptoms and cure the disease. However, for chronic diseases treatment, chronic patients need long-term medication, organic solvents, and surfactants in the preparation will bring a series of adverse reactions and side effects. Compared with the ethanol/Cremophor solution formulation, although the
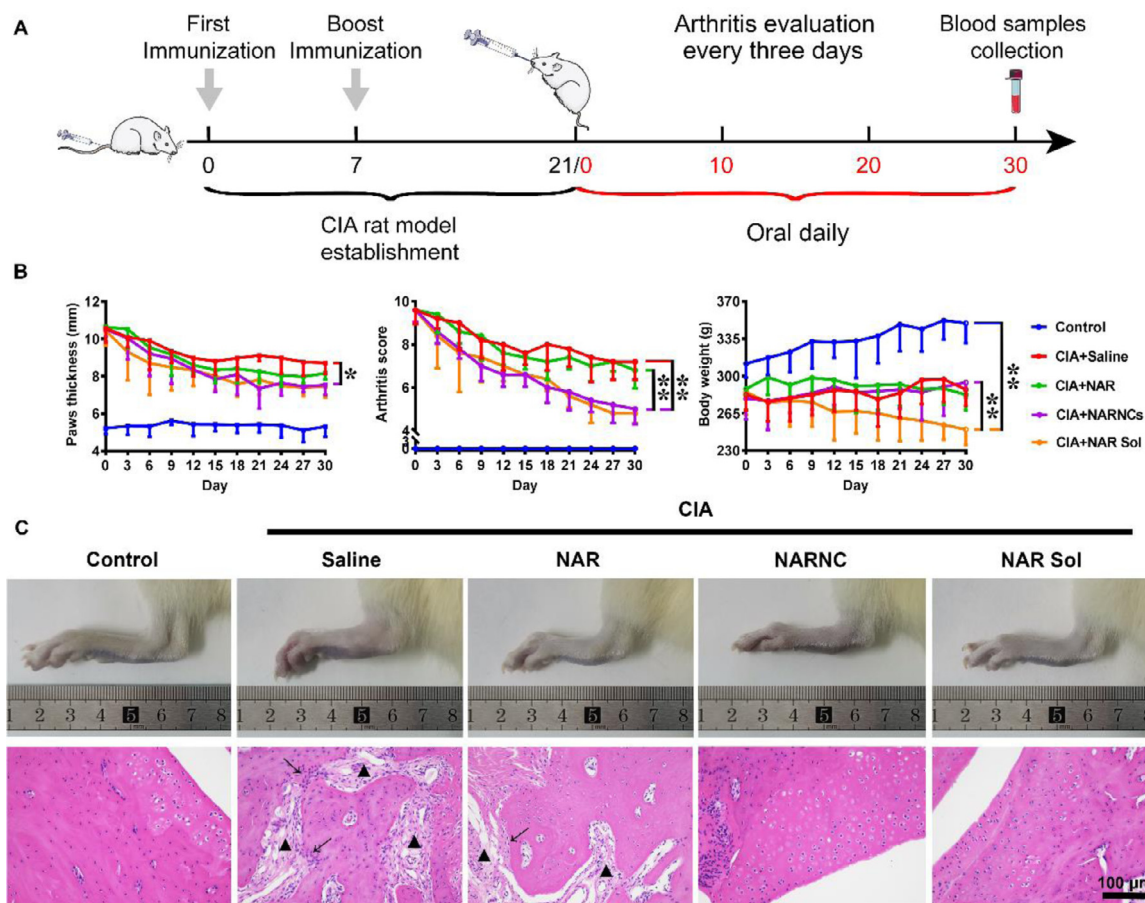
Fig. 7 – *In vivo* anti-inflammatory effects of NAR. (A) Schematic of CIA rat model establishment and treatment programs. (B) Paw thickness, arthritis scores, and body weights of the rats recorded every 3 d (C) Photographs of hind paws (upper row) and histological analysis with hematoxylin-eosin staining of ankle joint tissues (lower row) after treatment with saline, NAR suspension, NARNCs, and NAR Sol. Arrows show inflammatory cell infiltration; the triangle denotes cell death. Data are presented shown as mean ± SD, $n = 5$, *$P < 0.05$, **$P < 0.01$.

preparation of NCs is slightly complex and the cost is a bit high, almost negligible surfactants and/or polymers used in the formulation will not bring safety concerns and can be used for long-term administration [14,36]. Despite the oral bioavailability of NARNCs is lower than the solution, it may be critical sufficient to make a NAR, a poorly water-soluble drug, clinically effective.

4.   Conclusion

In this study, NARNCs stabilized by F127 were successfully prepared by wet milling. During the milling process, the crystal state of NAR was unchanged, and no obvious interaction occurred between NAR and F127. NARNCs also showed superior dissolution, favorable cellular uptake, improved transcellular ability, and significantly enhanced oral bioavailability and anti-inflammatory efficacy. Notably, the improved therapeutic effects are not compromised by apparent side effects because NARNCs contain no organic solvents. Therefore, NARNCs prepared by wet milling have broad application prospects in the treatment of RA.

Conflicts of interest

The authors report no conflicts of interest. The authors alone are responsible for the content and writing of this article.

Acknowledgments

Supplementary materials

Supplementary material associated with this article can be found, in the online version, at doi:10.1016/j.ajps.2021.09.001.

REFERENCES

[1] Qindeel M, Ullah MH, Fakhar Ud D, Ahmed N, Rehman AU. Recent trends, challenges and future outlook of transdermal drug delivery systems for rheumatoid arthritis therapy. J Control Release 2020;327:595–615.

[2] Hughes SD, Ketheesan N, Haleagrahara N. The therapeutic potential of plant flavonoids on rheumatoid arthritis. Crit Rev Food Sci Nutr 2017;57(17):3601–13.

[3] Crofford LJ. Use of NSAIDs in treating patients with arthritis. Arthritis Res Ther 2013;15:10.

[4] Roubille C, Richer V, Starnino T, Mccourt C, Mcfarlane A, Fleming P, et al. The effects of tumour necrosis factor inhibitors, methotrexate, non-steroidal anti-inflammatory drugs and corticosteroids on cardiovascular events in rheumatoid arthritis, psoriasis and psoriatic arthritis: a systematic review and meta-analysis. Ann Rheum Dis 2015;74(3):480–9.

[5] Divonne MD, Gottenberg JE, Salliot C. Safety of biologic DMARDs in RA patients in real life: a systematic literature review and meta-analyses of biologic registers. Joint Bone Spine 2017;84(2):133–40.

[6] Teng J, Li YL, Yu WZ, Zhao YL, Hu XQ, Tao NP, et al. Naringenin, a common flavanone, inhibits the formation of AGEs in bread and attenuates AGEs-induced oxidative stress and inflammation in RAW264.7 cells. Food Chem 2018;269:35–42.

[7] Renugadevi J, Prabu SM. Cadmium-induced hepatotoxicity in rats and the protective effect of naringenin. Exper Toxi Path 2010;62(2):171–81.

[8] Cui WX, He ZH, Zhang YT, Fan QY, Feng NP. Naringenin cocrystals prepared by solution crystallization method for improving bioavailability and anti-hyperlipidemia effects. AAPS PharmSciTech 2019;20(3):12.

[9] Subramani T, Ganapathyswamy H. An overview of liposomal nano-encapsulation techniques and its applications in food and nutraceutical. J Food Sci Technol-Mysore 2020;57(10):3545–55.

[10] Zou LQ, Zheng BJ, Zhang RJ, Zhang ZP, Liu W, Liu CM, et al. Influence of lipid phase composition of excipient emulsions on curcumin solubility, stability, and bioaccessibility. Food Biophys 2016;11(3):213–25.

[11] Ishimoto K, Miki S, Ohno A, Nakamura Y, Otani S, Nakamura M, et al. Beta-Carotene solid dispersion prepared by hot-melt technology improves its solubility in water. J Food Sci Technol-Mysore 2019;56(7):3540–6.

[12] Homayouni A, Amini M, Sohrabi M, Varshosaz J, Nokhodchi A. Curcumin nanoparticles containing poloxamer or soluplus tailored by high pressure homogenization using antisolvent crystallization. Int J Pharm 2019;562:124–34.

[13] Shakeel F, Haq N, Siddiqui NA, Alanazi FK, Alsarra IA. Solubility and thermodynamic behavior of vanillin in propane-1, 2-diol + water cosolvent mixtures at different temperatures. Food Chem 2015;188:57–61.

[14] Singhal M, Baumgartner A, Turunen E, Van Veen B, Hirvonen J, Peltonen L. Nanosuspensions of a poorly soluble investigational molecule ODM-106: impact of milling bead diameter and stabilizer concentration. Int J Pharm 2020;587.

[15] Kapoor R, Pathak S, Najmi AK, Aeri V, Panda BP. Processing of soy functional food using high pressure homogenization for improved nutritional and therapeutic benefits. Inno Food Sci Emer Tech 2014;26:490–7.

[16] Quinn K, Gullapalli RP, Merisko-Liversidge E, Goldbach E, Wong A, Liversidge GG, et al. A formulation strategy for gamma secretase inhibitor ELND006, a BCS class II compound: development of a nanosuspension formulation with improved oral bioavailability and reduced food effects in dogs. J Pharm Sci 2012;101(4):1462–74.

[17] Li F, Li LS, Wang SN, Yang Y, Li J, Liu DC, et al. Improved dissolution and oral absorption by co-grinding active drug probucol and ternary stabilizers mixtures with planetary beads-milling method. Asian J Pharm Sci 2019; 14(6):649–57.

[18] Guo MR, Dong YJ, Wang YZ, Ma MC, He ZG, Fu Q. Fabrication, characterization, stability and in vitro evaluation of nitrendipine nanocrystals by media milling. Powder Technol 2019;358:20–8.

[19] Kruger J, Sus N, Frank J. Ascorbic acid, sucrose and olive oil lipids mitigate the inhibitory effects of pectin on the bioaccessibility and Caco-2 cellular uptake of ferulic acid and naringenin. Food Funct 2020;11(5):4138–45.

[20] Kusaka T, Nakayama M, Nakamura K, Ishimiya M, Furusawa E, Ogasawara K. Effect of silica particle size on macrophage inflammatory responses. PLoS ONE 2014;9(3):9.

[21] Yang XY, Wang J, Zhou ZW, Jiang R, Huang J, Chen LL, et al. Silica-induced initiation of circular ZC3H4 RNA/ZC3H4 pathway promotes the pulmonary macrophage activation. Faseb J 2018;32(6):3264–77.

[22] Couto M, Cates C. Laboratory guidelines for animal care. Meth molecu biology 2019;1920:407–30.

[23] Wang YW, Wang SC, Firempong CK, Zhang HY, Wang MM, Zhang Y, et al. Enhanced solubility and bioavailability of naringenin via liposomal nanoformulation: preparation and in vitro and in vivo Evaluations. AAPS PharmSciTech 2017;18(3):586–94.

[24] Xu Y, Chen Z, Xu Z, Du Y, Han J, Yuan X, et al. Intra-Articular injection of acid-sensitive stearoxyl-ketal-dexamethasone microcrystals for long-acting arthritis therapy. Asian J Pharm Sci 2020.

[25] Patel CM, Chakraborty M, Murthy ZVP. Preparation of fenofibrate nanoparticles by combined stirred media milling and ultrasonication method. Ultra Sono 2014;21(3):1100–7.

[26] Liu P, Rong XY, Laru J, Van Veen B, Kiesvaara J, Hirvonen J, et al. Nanosuspensions of poorly soluble drugs: preparation and development by wet milling. Int J Pharm 2011;411(1–2):215–22.

[27] Merisko-Liversidge E, Liversidge GG, Cooper ER. Nanosizing: a formulation approach for poorly-water-soluble compounds. Eur J Pharm Sci 2003;18(2):113–20.

[28] Guo MR, Wei MD, Li W, Guo MC, Guo CL, Ma MC, et al. Impacts of particle shapes on the oral delivery of drug nanocrystals: mucus permeation, transepithelial transport and bioavailability. J Control Release 2019;307:64–75.

[29] Teeranachaideekul V, Junyaprasert VB, Souto EB, Mueller RH. Development of ascorbyl palmitate nanocrystals applying the nanosuspension technology. Int J Pharm 2008;354(1–2):227–34.

[30] Jha DK, Shah DS, Amin PD. Thermodynamic aspects of the preparation of amorphous solid dispersions of Naringenin with enhanced dissolution rate. Int J Pharm 2020;583:12.

[31] Yousaf AM, Kim DW, Kim DS, Kim JO, Youn YS, Cho KH, et al. Influence of polyvinylpyrrolidone quantity on the solubility, crystallinity and oral bioavailability of fenofibrate in solvent-evaporated microspheres. J Microencapsul 2016;33(4):365–71.

[32] Lu Y, Lin M, Zong J, Zong L, Zhao Z, Wang S, et al. Highly bioavailable curcumin preparation with a co-grinding and solvent-free process. Food Sci Nut 2020;8(12):6415–25.

[33] Mishra V, Nayak P, Yadav N, Singh M, Tambuwala MM, AaA Aljabali. Orally administered self-emulsifying drug delivery system in disease management: advancement and patents. Expert Opin Drug Deli 2020.

[34] Peng C, Lei JX. Compatible stability of methylprednisolone sodium succinate and tropisetron in 0.9% sodium chloride injection. Eur J Hos Pharm Sci and Practice 2020;27(E1):E58–62.

[35] Chen P, Chen F, Lei J, Zhou B. Physical compatibility and chemical stability of fentanyl and naloxone hydrochloride in 0.9% sodium chloride injection solution for patient-controlled analgesia administration. Drug Design Dev The 2020;14:4179–87.

[36] Kayser O, Olbrich C, Yardley V, Kiderlen AF, Croft SL. Formulation of amphotericin B as nanosuspension for oral administration. Int J Pharm 2003;254(1):73–5.